ADVANCED OPTICAL MATERIALS
www.advopticalmat.de

Effective Out-Of-Plane Thermal Conductivity of Silicene by Optothermal Raman Spectroscopy

Eleonora Bonaventura, Daya. S. Dhungana, Chiara Massetti, Jacopo Pedrini, Carlo Grazianetti, Christian Martella, Fabio Pezzoli, Alessandro Molle,* and Emiliano Bonera**

Silicene has recently been revisited as a 2D material with potential thermoelectric applications. Here, the thermal properties of supported silicene are determined by optothermal Raman spectroscopy. Single and multilayer silicene is grown either directly on silver (Ag) substrates or on an intermediate tin (Sn) monolayer, introduced to reduce the influence of the substrate on the physical properties of silicene. Experimental values of an effective cross-plane thermal conductivity of 0.5 W/mK are obtained for silicene on Ag and 0.3 W/mK for silicene on stanene-Ag. The values of the interfacial thermal conductance, on the other hand, are 0.3 and 0.5 GW/m^{2}K, respectively. Heterostack engineering is confirmed as a versatile strategy for extracting relevant physical parameters in silicene and for modulating the thermal response in the 2D limit.

1. Introduction

Silicene, the 2D form of silicon (Si), has been showing great promise for technological applications since its discovery.[1,2] Driven by the intrinsic compatibility with the semiconductor technology and the peculiar band structure – which can host Dirac electrons as graphene – research based on silicene has been ever evolving.[3] However, despite advances in growth and processes that bring the 2D Si allotrope closer to integration into functional devices,[4,5] substrate requirements remain an open issue. The (111)-terminated silver surface is the most used template for the experimental realization of silicene. A stanene buffer layer can also be grown on this substrate, which has been shown to favor decoupling between silicene and Ag.[6,7] An in-depth knowledge of the properties of the interface between the silicene and the support or protective layers is therefore essential to facilitate the development of emerging technologies.

Recently, silicene has been proposed as a valuable candidate for thermoelectric applications.[8] Thermoelectric devices allow for the direct conversion of heat into electrical energy and vice versa. A thermoelectric generator could effectively increase energy efficiency and reduce greenhouse gas emissions using waste heat as a power source. The applicable scenarios for thermoelectrics can include transportation, extreme environments, electronics, and sensors.[9,10] The conversion efficiency of a thermoelectric material is quantified by the dimensionless figure of merit $zT = (\alpha^2 \sigma)T/k$ where α, σ, k, T are Seebeck coefficient, electrical conductivity, thermal conductivity, and absolute temperature. Boosting zT (>1), which is inversely proportional to the inherent thermal conductivity, is a key requirement for the design of advanced thermoelectric materials.[11] On top of this technology evolution, the cross-plane heat transfer, which is directly related to critical aspects of exploiting properties in new nanomaterials such as heat dissipation, energy consumption and conversion, is scarcely explored in silicon at the 2D level, that is, at a targeted body thickness relevant to produce electronic devices.

The number of theoretical works reporting on the thermal conductivity of silicene is extremely small, in contrast to the range of calculated values. Furthermore, to the best of our knowledge, the thermal properties of silicene have not been investigated experimentally due to the lack of suitable configurations. Molecular dynamics simulations based on classical potentials developed for bulk silicon yield values in the range of 20 to 40 W/mK.[12–14] Using first-principles calculations, Xie et al.[15] obtain 9.4 W/mK for monolayer silicene. A similar result is also highlighted by Zhang and co-workers by applying different computational methods.[16] In another work, the thermal conductivity is reported for free-standing silicene and its supported form.[17] When silicene is modeled on a SiO_2 substrate, a decrease in thermal conductivity is suggested. Wang et al. explain this effect in terms of reduced phonon relaxation times.

E. Bonaventura, J. Pedrini, F. Pezzoli, E. Bonera
Department of Materials Science
Università degli Studi di Milano-Bicocca
Via R. Cozzi 55, Milan 20125, Italy
E-mail: eleonora.bonaventura@unimib.it; emiliano.bonera@unimib.it
E. Bonaventura, D. S. Dhungana, C. Massetti, C. Grazianetti, C. Martella, A. Molle
CNR-IMM, Unit of Agrate Brianza
via C. Olivetti 2, Agrate Brianza 20864, Italy
E-mail: alessandro.molle@cnr.it

The ORCID identification number(s) for the author(s) of this article can be found under https://doi.org/10.1002/adom.202401466

DOI: 10.1002/adom.202401466

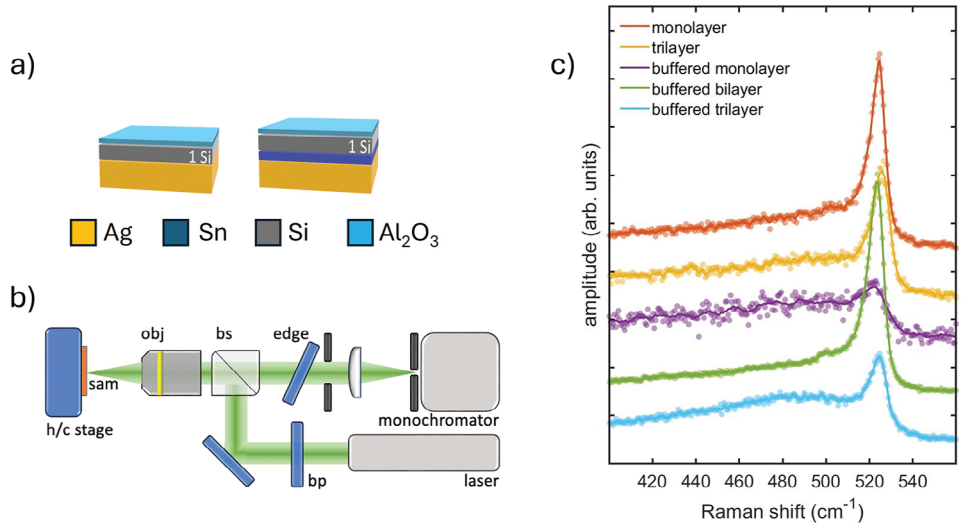

Figure 1. a) Sketch of the silicene-based configurations used in this work. From left to right: directly grown silicene and buffered silicene. All samples are deposited on Ag(111) substrate. The relative thickness is not to scale. b) Scheme of the optical system used for the optothermal Raman measurements. bp: band pass filter, bs: beam splitter; obj: objective; edge: edge pass filter. c) Raman spectra at low temperature, obtained with a low incident laser power.

Here, we report on the investigation of the thermal response of supported silicene using an optothermal method based on Raman spectroscopy. Two different configurations were considered: silicene directly grown on silver and silicene grown on a stanene buffer layer. The optothermal Raman technique relies on a direct relationship between the Raman signal and the temperature. In fact, the phonon frequencies and lifetimes, induced by the anharmonicity in the interatomic potentials, are temperature dependent, and so are also the intensity, frequency, and width of the corresponding Raman peak. Using the same incident radiation to locally heat the system, non-contact thermal measurements can be performed.[18–21] The thermal conductivity can indeed be extracted by quantifying the Raman shift. This approach can be readily applied to silicene, which exhibits a characteristic Raman spectrum in both its single- and multi-layer forms when properly stabilized.[22] Although the atomic scale control and quantum confinement effects can generally affect the thermoelectric performance in a nanomaterial,[23,24] configuring silicene in diverse heterostructure schemes allows us to quantify some pivotal thermoelectric quantities in real cases.

2. Results and Discussion

2.1. Growth and Characterization

We explore epitaxial silicene in the form of single- and multilayers. All the samples are supported by an Ag(111) epilayer on mica. The silicene layers have been grown directly on silver and on a 2D tin buffer layer (termed stanene). While the direct growth results in a 2D polycrystalline texture, stanene buffering leads to a single-phase formation eventually giving rise to a silicene-stanene heterostacked structure.[6,7] Silicene and silicene-stanene layers have been deposited by molecular beam epitaxy on Ag(111) substrates, as described in more detail in the experimental section. The single layer of silicene on Ag(111) is therefore a mixture of 4×4, $\sqrt{13}\times\sqrt{13}\,R13.9°$, $2\sqrt{3}\times2\sqrt{3}\,R30°$, while $\sqrt{3}\times\sqrt{3}$ single phase is stabilized for multilayer silicene and silicene-stanene configurations. One and three layers of silicene were considered for direct growth on Ag, while one, two, and three layers were considered for the stanene-Ag substrate. We will refer to the latter as the "buffered" samples. A 5 nm-thick Al_2O_3 encapsulating layer was deposited on all the samples for protection against oxidation. A sketch of directly grown and buffered silicene is shown in **Figure 1a**.

Raman spectroscopy in backscattering configuration was performed using a hot-cold stage to control the temperature of the sample as in Figure 1b. The 532 nm incident laser power was kept below 3 mW. The room-temperature spectra in Figure 1c show the typical asymmetrical shape. For silicene, the Raman spectrum can be described as a superposition of two components. The most intense peak is centered at ≈520 cm^{-1}. It corresponds to the E_{2g} mode of the hexagonal Si rings in monolayer silicene. The other one is broader and is located at lower wavenumbers (480–500 cm^{-1}). This feature is related to the intrinsic disorder of the bidimensional structure or to unresolved breathing modes.[25] The outcomes of the Raman analysis are consistent with the previously reported Raman data of supported single and multilayer silicene.[26,27] The sharp and intense Raman band of silicene can thus be used to probe and quantify its thermal response in the diverse silicene layouts.

2.2. Temperature and Raman Spectrum

The first step for investigating the thermal properties of supported silicene is to determine the temperature dependence of its Raman spectrum. The two silicene-based configurations (directly grown and buffered) were measured at constant incident light power (P) by varying the external temperature (T) between 123 and 423 K. P was kept low to avoid alteration of the

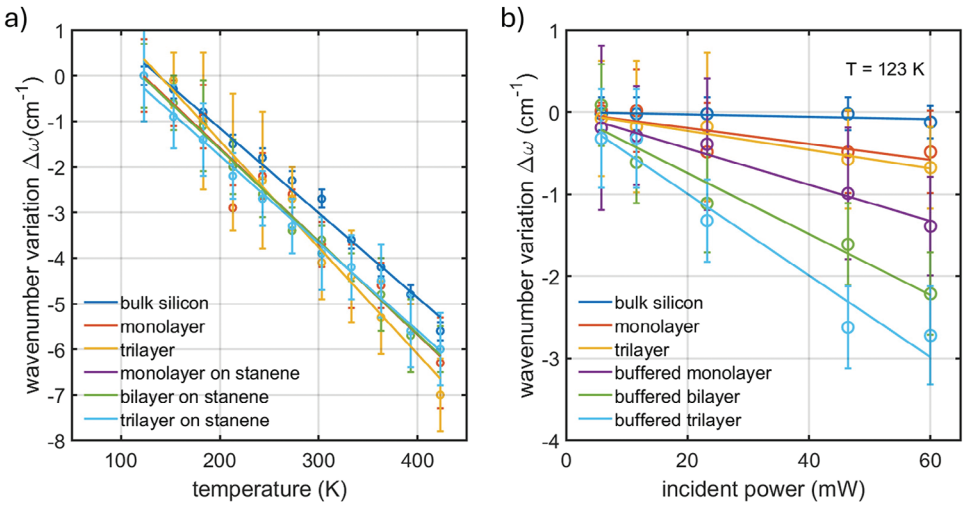

Figure 2. a) Wavenumber variation in the Raman peak of silicene as a function of temperature T. The fixed incident power P is 5.8 mW. b) Wavenumber change in the Raman band of silicene as a function of the incident power P. All the measurements were taken with the samples cooled at 123 K.

spectra due to illumination-induced local heating. The positions of the Raman peaks were obtained by fitting a pseudo-Voigt function to the experimental data. In addition to silicene, a bulk silicon reference was also measured under the same experimental conditions. In the temperature range under consideration, the wavenumber variation $\Delta\omega$(T) follows the linear trend already reported for other supported 2D materials.[28–30] The linearity in the Raman peak position as a function of the temperature is shown in **Figure 2**a. The proportionality constant $\chi = d\omega/dT$, obtained from the linear fit, amounts to -0.020 cm^{-1} K^{-1} for all the samples. The thermal coefficient χ, which is larger in modulus than that reported in the literature for a single layer of silicene grown on Ag,[31] appears to be independent of the stacking and compatible with the value obtained for bulk silicon.

2.3. Thermal Properties of the Stacks

According to the Fourier theory, the coherence length of the phonons is assumed to be smaller than the thickness of the material.[32] However, this condition breaks down in case of an atomically thin layer. Nonetheless, the Fourier description has been effectively adopted to interpret the heat conduction in 2D materials like black phosphorus and therein infer the relevant thermal characteristics.[18,33,34] Phenomenologically, the heat transfer in a medium can be described by Fourier's law:

$$q = -k\nabla T \tag{1}$$

Equation (1) relates the heat flow density q through a surface to the temperature gradient ∇T. The proportionality constant k is the integral thermal conductivity.The study presented here involves multilayered structures from the stacking of different materials. Let us first consider the simplest configuration of a silicene layer of thickness t_{Si} grown on Ag(111).

Given that the lateral dimension is on the order of millimetres, we model the silicene and silicene-stanene stacks as infinitely extended in the plane. In order to extract an effective value for the thermal conductivity of silicene, we consider the substrate as a constant temperature thermal bath because k_{Ag} is ≈430 W/mK,[35] i.e. much larger than the one expected from the silicene.[15–17] The alumina capping layer is 5 nm thick with a thermal conductivity of the order of 1–3 W/mK, and therefore its contribution to the heat dispersion can be reasonably disregarded.[36,37] Similar considerations hold for convection and irradiation processes. The ultra-scaled thickness of silicene also suggests that in-plane heat transport is negligible. The presence of grain boundaries (as well as other defects) can indeed provide scattering centers for phonons and carriers.[38–40] Therefore, by considering a homogeneously constant substrate temperature, to a first approximation we can describe the laser-induced local temperature variation as only depending on the thermal conductivity of silicene k_{Si}, and on the interface thermal conductance G between silicon and Ag. We can treat the temperature gradient as one-directional effect, that is, $\nabla T \rightarrow \frac{dT}{dz}$ with z pointing out to the normal direction of the stack. In terms of heat dissipation and conduction, the silicene samples can be described as a series of a thermal resistances of the body and the interface(s), in analogy with the electrical circuit. By specifying the elements of the system under investigation and neglecting the substrate contribution, the linear dependence of ΔT on Δq becomes:

$$\Delta T = \left[\frac{t_{Si}}{k_{Si}} + \frac{1}{G}\right]\Delta q \tag{2}$$

where ΔT is the temperature change recorded by the Raman measurement, while Δq is the power density absorbed by the silicene layer, which can instead be extracted by measuring the optothermal Raman effect as a function of the incident laser power P. The temperature variation ΔT is also linearly related to the thickness of silicene. For silicene directly grown on Ag, G is the actual interfacial thermal conductance of the Si-Ag interface (G_{SiAg}). For the heterostructures of silicene on stanene-Ag, G is the resultant of different terms: $1/G = 1/G_{SiSn} + t_{Sn}/k_{Sn} + 1/G_{SnAg}$, where G_{SiSn} and G_{SnAg} are the Si-Sn and Sn-Ag interfacial thermal

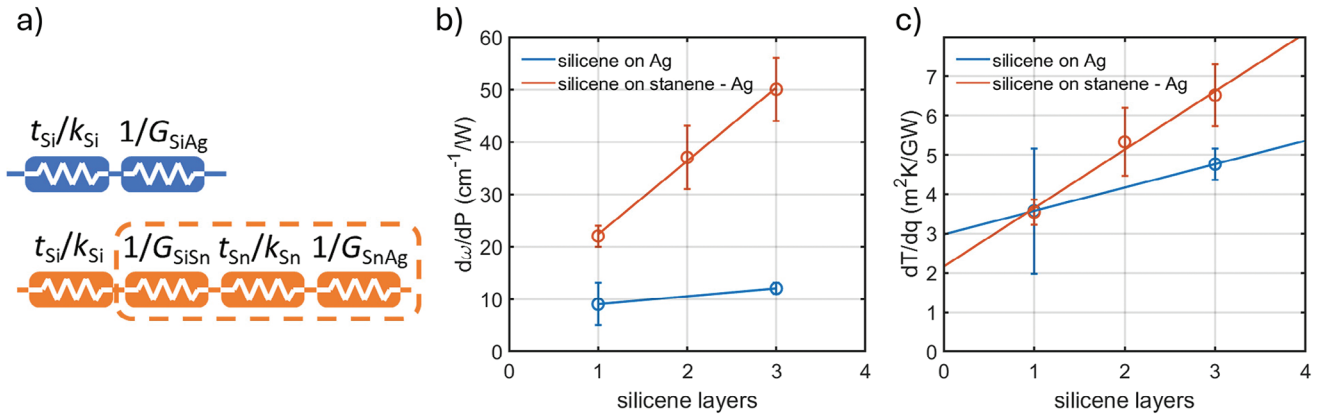

Figure 3. a) Equivalent thermal circuit for directly grown (top) and buffered (bottom) silicene. b) dω/dP as a function of the number of silicene layers. c) dT/dq as a function of the number of silicene layers. Blue color is used for silicene on Ag, while orange indicates the silicene on stanene-Ag configuration.

conductances, while k_{Sn} and t_{Sn} are the thermal conductivity and the thickness of the stanene layer, respectively.

In our experiment, we cannot separate the contributions from the different interfaces in the heterostructure, and therefore the extracted G will be an effective value.

2.4. Experimental Determination of k and G

A number of Raman spectra were collected at different incident laser powers and converted to the local temperature rise at the laser spot using the previously obtained temperature coefficients. This highly localized power induces a change in temperature that can be deduced from the Raman shift variation $\Delta\omega$. To display Raman shifts more evidently even with low incident power P, we set the external temperature at 123 K. At higher base temperatures, the local changes in $\Delta\omega$ are evident only at higher excitation intensities. The evolution of $\Delta\omega$ as a function of P for all the samples is shown in Figure 2b. Bulk silicon, used as reference, does not show any change with varying P, because of the heat dissipation deep through the bulk wafer. In fact, its thermal conductivity is 142 W/mK at room temperature.[41] The silicene samples, however, show that a higher P corresponds to large $\Delta\omega$, and hence a higher local temperature. We also notice that the slopes dω/dP are sample-dependent, thus suggesting a role of the thickness and of the stanene layer in the absorption and the dissipation process. For comparison, in a previously published paper we reported a similar power dependence on a detached silicene sample.[5] In Figure 2b the dissipation of heat is more effective, probably because of the better crystalline quality of the stack.

For the determination of the thermal properties the simplified model described in the previous section and schematized in the drawing of **Figure** 3a is used. To get a quantitative description, in Figure 3b we plot the slope dω/dP as a function of the number of silicene layers. An increase of the thickness is associated with an increase of the slope. The corresponding change in T cannot be directly related to the thermal properties because the power absorption changes with the structural details of each sample. The absorbed laser power for each configuration can be estimated as: $P_{Abs} = A{\cdot}P$ where A is the absorbance of the silicene-based structures. Since the wavelength used for the Raman characterization is below the plasma edge of the Ag substrate, the light is almost completely reflected, and the substrate absorption is about zero.[42] In addition, the thin amorphous Al_2O_3 capping layer is optically transparent and no contribution is expected from it.[43] Therefore, we assume the absorption of silicene-based samples equal to $1\text{-}R$ where the reflectivity R can be measured with a standard spectrophotometer as reported in ref. [19] In this framework, Figure 3b can thus be replotted as Figure 3c by changing $d\omega/dP$ into dT/dq trough the relation:

$$\frac{\Delta T}{\Delta q} = \frac{d\omega}{dP_{Abs}} S\chi^{-1} \tag{3}$$

where S is the illuminated area as calculated from the diffraction limited diameter of the focus as $\lambda/2$ N.A. (N.A. is the numerical aperture), and χ^{-1} is the thermal coefficient obtained from the data in Figure 2a. Reading the linear dependence in Figure 3c in a Fourier picture of a homogeneous layer on top of a substrate, the linear plot is an angular coefficient of t_{mono}/k where t_{mono} is the thickness of a monolayer of silicene, while the intercept is $1/G$. The thermal conductivity values obtained with an average silicene thickness of 0.31 nm are 0.5 W/mK for the Si/Ag set and 0.3 W/mK for the Si/Sn/Ag set.[4,44] Our values, which are lower than the thermal conductivity of bulk silicon, are compatible with those reported for low-dimensional Si-based systems.[24] From the point of view of the interfacial thermal conductance the values extracted for the Si/Ag and Si/Sn/Ag configurations are 0.3 and 0.5 GW/m^{2}K, respectively. The stanene buffering turns out to reduce the thermal flow from the sample to the substrate, resulting in a higher thermal conductivity of the 2D body. As mentioned above, these values can only be read as equivalent quantities within the assumed approximations (the application of the Fourier analysis and the coexistence of multiple layers).

3. Conclusion

In summary, we have investigated the thermal response of silicene grown directly on Ag(111) and buffered by a layer of stanene. Using the optothermal Raman method, we measured the change in Raman shift as a function of stack temperature for mono- and multi-layer silicene to calibrate the

Raman shift as a local thermometer. We then measured the increase in local temperature by heating the samples with the excitation laser itself. We interpreted the change in terms of the effective value of the thermal conductivity and the interfacial thermal conductance, returning their experimental values: 0.5 W/mK and 0.3 GW/m^{2}K for silicene on Ag, 0.3 W/mK and 0.5 GW/m^{2}K for silicene on stanene-Ag. This is one of the first attempts to characterize the thermal behavior of epitaxial silicene. Although knowledge of electrical conductivity is essential for the correct definition of the merit factor zT, access to the thermal properties of silicene opened a new path for exploring its thermoelectric applications. With the aim of finding a way to single out the properties of the silicene layers from the substrate, we also observed a variation of the thermal characteristics as a function of the introduction of a monolayer stanene spacer. Heterostack engineering thus proved to be a versatile strategy for modulating the effective thermal response of silicene at the 2D limit.

4. Experimental Section

Growth: Silicene samples were epitaxially grown, on commercially available 300 nm thick Ag(111) substrates, in a Lab10 MBE system (supplied from Scienta Omicron GmbH) under ultra-high vacuum conditions. The base pressure was kept $<10^{-10}$ mbar. Before the thin film depositions, the Ag surface was pretreated by cycles of Ar+ sputtering, followed by annealing at 550 °C. Standard k-cell and a silicon sublimator were used for the Sn and Si deposition, respectively. Single and multi-layers silicene were grown on two surface templates: the bare Ag(111) and the stanene on Ag(111). According to the growth scheme in ref. [6] the silicene-stanene heterostructures were realized starting with the deposition of 1.33 monolayer Sn on Ag(111). Silicene and stanene thicknesses were determined by calibration of the silicon/tin flux using a thickness monitor and by post-growth probing by means of in situ low energy electron diffraction and Auger electron spectroscopy. Finally, before removing the samples from the vacuum, a 5 nm non-reactive Al_2O_3 capping layer was applied to prevent oxidation in ambient conditions.[22]

Raman Measurements: Temperature dependent Raman measurements were performed using a system based on a Horiba T64000 in a backscattering configuration with an edge filter. A 532 nm laser was focused on the sample surface by a long working distance 20x objective with a numerical aperture (N. A.) of 0.40. The samples were heated and cooled through a nitrogen purged thermal stage Linkam HFS-600. The energy loss due to the glass window of the thermal stage has been neglected. A neutral density filter at the laser output was used to control the power incident on the sample surface. The integration time of the Raman measurements was 15 s and 3 accumulations, the minimum values to obtain a detectable Raman signal from the silicene layers in this configuration. To better calibrate the temperature, a bulk silicon sample was introduced into the stage to provide a real-time reference for the temperature measurement.

Acknowledgements

This research was funded by European Commission within the H2020 research and innovation program under the ERC-COG 2017 Grant No. 772261 "XFab" and partially supported by the Italian Ministry of University and Research (MUR) under the PRIN 2020 Grant No. 2020RPEPNH "PHOTO". E.B. thanks the University of Milano Bicocca for funding (Bando Infrastrutture di Ricerca 2021). The authors would like to thank Riccardo Loss for help with the Raman measurements.

Conflict of Interest

The authors declare no conflict of interest.

Author Contributions

El.B. performed investigation, methodology, formal analysis, data handling, wrote the original draft; D.S.D. performed investigation, wrote the manuscript and contributed to the scientific discussion; C.M. wrote the manuscript, performed editing, visualization and contributed to the scientific discussion; J.P. wrote the manuscript and contributed to the scientific discussion; C.G. wrote the manuscript and contributed to the scientific discussion, Chr.M. wrote the manuscript and contributed to the scientific discussion; F.P. wrote the manuscript and contributed to the scientific discussion; A.M. performed conceptualization, wrote the manuscript and performed editing, supervision, project administration, and acquired funding. Em.B. performed conceptualization, methodology, formal analysis, visualization, wrote the original draft, performed supervision, project administration, and acquired funding.

Data Availability Statement

The data that support the findings of this study are available from the corresponding author upon reasonable request.

Keywords

2D materials, Raman spectroscopy, silicene, thermal properties, thermoelectrics, xenes

Received: May 30, 2024
Revised: August 1, 2024
Published online: August 27, 2024

[1] P. Vogt, P. De Padova, C. Quaresima, J. Avila, E. Frantzeskakis, M. C. Asensio, A. Resta, B. Ealet, G. L. Lay, *Phys. Rev. Lett.* **2012**, *108*, 155501.
[2] A. Molle, J. Goldberger, M. Houssa, Y. Xu, S.-C. Zhang, D. Akinwande, *Nat. Mater.* **2017**, *16*, 163.
[3] L. Matthes, O. Pulci, F. Bechstedt, *J. Phys.: Condens. Matter* **2013**, *25*, 395305.
[4] L. Tao, E. Cinquanta, D. Chiappe, C. Grazianetti, M. Fanciulli, M. Dubey, A. Molle, D. Akinwande, *Nat. Nanotechnol.* **2015**, *10*, 227.
[5] C. Martella, C. Massetti, D. S. Dhungana, E. Bonera, C. Grazianetti, A. Molle, *Adv. Mater.* **2023**, *35*, 2211419.
[6] D. S. Dhungana, C. Grazianetti, C. Martella, S. Achilli, G. Fratesi, A. Molle, *Adv. Funct. Mater.* **2021**, *31*, 2102797.
[7] S. Achilli, D. S. Dhungana, F. Orlando, C. Grazianetti, C. Martella, A. Molle, G. Fratesi, *Nanoscale* **2023**, *15*, 11005.
[8] B. Zhu, Q. Chen, S. Jiang, M. Holt, W. Zhu, D. Akinwande, L. Tao, *InfoMat* **2021**, *3*, 271.
[9] L. E. Bell, *Science* **2008**, *321*, 1457.
[10] D. Champier, *Energy Convers. Manag.* **2017**, *140*, 167.
[11] R. He, G. Schierning, K. Nielsch, *Adv. Mater. Technol.* **2018**, *3*, 1700256.
[12] H. Li, R. Zhang, *Europhys. Lett.* **2012**, *99*, 36001.
[13] M. Hu, X. Zhang, D. Poulikakos, *Phys. Rev. B* **2013**, *87*, 195417.
[14] Q.-X. Pei, Y.-W. Zhang, Z.-D. Sha, V. B. Shenoy, *J. Appl. Phys.* **2013**, *114*, 033526.
[15] H. Xie, M. Hu, H. Bao, *Appl. Phys. Lett.* **2014**, *104*, 131906.
[16] X. Zhang, H. Xie, M. Hu, H. Bao, S. Yue, G. Qin, G. Su, *Phys. Rev. B* **2014**, *89*, 054310.
[17] Z. Wang, T. Feng, X. Ruan, *J. Appl. Phys.* **2015**, *117*, 084317.
[18] E. Bonera, A. Molle, *Nanomaterials* **2022**, *12*, 1410.
[19] E. Bonaventura, D. S. Dhungana, C. Martella, C. Grazianetti, S. Macis, S. Lupi, E. Bonera, A. Molle, *Nanoscale Horiz.* **2022**, *7*, 924.

[20] H. Malekpour, A. A. Balandin, *J. Raman Spectrosc.* **2018**, *49*, 106.
[21] D. Tristant, A. Cupo, X. Ling, V. Meunier, *ACS Nano* **2019**, *13*, 10456.
[22] A. Molle, G. Faraone, A. Lamperti, D. Chiappe, E. Cinquanta, C. Martella, E. Bonera, E. Scalise, C. Grazianetti, *Faraday Discuss.* **2021**, *227*, 171.
[23] L. D. Hicks, M. S. Dresselhaus, *Phys. Rev. B* **1993**, *47*, 16631.
[24] A. I. Boukai, Y. Bunimovich, J. Tahir-Kheli, J.-K. Yu, W. A. Goddard III, J. R. Heath, *Nature* **2008**, *451*, 168.
[25] E. Scalise, E. Cinquanta, M. Houssa, B. V. D. Broek, D. Chiappe, C. Grazianetti, G. Pourtois, B. Ealet, A. Molle, M. Fanciulli, V. V. Afanas'Ev, A. Stesmans, *Appl. Surf. Sci.* **2014**, *291*, 113.
[26] E. Cinquanta, E. Scalise, D. Chiappe, C. Grazianetti, B. van den Broek, M. Houssa, M. Fanciulli, A. Molle, *J. Phys. Chem. C* **2013**, *117*, 16719.
[27] C. Grazianetti, E. Cinquanta, L. Tao, P. De Padova, C. Quaresima, C. Ottaviani, D. Akinwande, A. Molle, *ACS Nano* **2017**, *11*, 3376.
[28] I. Calizo, A. A. Balandin, W. Bao, F. Miao, C. N. Lau, *Nano Lett.* **2007**, *7*, 2645.
[29] A. Łapińska, A. Taube, J. Judek, M. Zdrojek, *J. Phys. Chem. C* **2016**, *120*, 5265.
[30] A. S. Pawbake, M. S. Pawar, S. R. Jadkar, D. J. Late, *Nanoscale* **2016**, *8*, 3008.
[31] D. Solonenko, O. D. Gordan, G. L. Lay, H. Sahin, S. Cahangirov, D. R. T. Zahn, P. Vogt, *2D Mater.* **2016**, *4*, 015008.
[32] D. G. Cahill, W. K. Ford, K. E. Goodson, G. D. Mahan, A. Majumdar, H. J. Maris, R. Merlin, S. R. Phillpot, *J. Appl. Phys.* **2003**, *93*, 793.
[33] T. Wang, R. Wang, P. Yuan, S. Xu, J. Liu, X. Wang, *Adv. Mater. Interfaces* **2017**, *4*, 1700233.
[34] Z. Luo, J. Maassen, Y. Deng, Y. Du, R. P. Garrelts, M. S. Lundstrom, P. D. Ye, X. Xu, *Nat. Commun.* **2015**, *6*, 8572.
[35] J. F. Shackelford, W. Alexander, *CRC Materials Science and Engineering Handbook*, CRC Press, Boca Raton, FL **2000**.
[36] B. Su-Yuan, T. Zhen-An, H. Zheng-Xing, Y. Jun, W. Jia-Qi, *Chin. Phys. Lett.* **2008**, *25*, 593.
[37] A. Cappella, J. Battaglia, V. Schick, A. Kusiak, A. Lamperti, C. Wiemer, B. Hay, *Adv. Eng. Mater.* **2013**, *15*, 1046.
[38] H. Dong, B. Wen, R. Melnik, *Sci. Rep.* **2014**, *4*, 7037.
[39] M. Khalkhali, A. Rajabpour, F. Khoeini, *Sci. Rep.* **2019**, *9*, 5684.
[40] X. Liu, J. Gao, G. Zhang, J. Zhao, Y.-W. Zhang, *ACS Omega* **2020**, *5*, 17416.
[41] C. J. Glassbrenner, G. A. Slack, *Phys. Rev.* **1964**, *134*, A1058.
[42] P. B. Johnson, R. W. Christy, *Phys. Rev. B* **1972**, *6*, 4370.
[43] C. Grazianetti, S. De Rosa, C. Martella, P. Targa, D. Codegoni, P. Gori, O. Pulci, A. Molle, S. Lupi, *Nano Lett.* **2018**, *18*, 7124.
[44] A. Resta, T. Leoni, C. Barth, A. Ranguis, C. Becker, T. Bruhn, P. Vogt, G. L. Lay, *Sci. Rep.* **2013**, *3*, 2399.